Journal of Molecular Catalysis A: Chemical 319 (2010) 78–84

Contents lists available at ScienceDirect

Journal of Molecular Catalysis A: Chemical

journal homepage: www.elsevier.com/locate/molcata

The impact of silver modification on the catalytic activity of iodine-doped titania for *p*-chlorophenol degradation under visible-light irradiation

Zhiqiao He[a], Lei Xie[a], Shuang Song[a,*], Cheng Wang[a], Jinjun Tu[a], Fangyue Hong[a], Qi Liu[b], Jianmeng Chen[b], Xinhua Xu[c]

[a] College of Biological and Environmental Engineering, Zhejiang University of Technology, Hangzhou 310032, People's Republic of China
[b] Institute of Environmental Science and Engineering, Zhejiang University of Technology, Hangzhou 310032, People's Republic of China
[c] Department of Environmental Engineering, Zhejiang University, Hangzhou 310027, People's Republic of China

ARTICLE INFO

Article history:
Received 25 August 2009
Received in revised form
27 November 2009
Accepted 7 December 2009
Available online 16 December 2009

Keywords:
Photodegradation
Titanium dioxide
Silver
Iodine
4-Chlorophenol

ABSTRACT

Iodine-doped titania photocatalysts (I-TiO_2) were improved by doping the catalysts with different contents of silver (Ag-I-TiO_2) to investigate the effect of silver modification on the structure and activity of the photocatalysts. The chemical and physical properties of the catalysts were determined by X-ray diffraction (XRD), the Brunauer–Emmett–Teller (BET) method, transmission electron microscopy (TEM), selected area electron diffraction pattern (SAED), X-ray photoelectron spectroscopy (XPS), and UV–vis diffuse reflectance spectra. The impact of silver modification on the photocatalytic activity was investigated via the photodegradation of *p*-chlorophenol (PCP) under visible-light irradiation. The significant enhancement of PCP degradation using Ag-I-TiO_2, with an optimum silver content of 3% can be ascribed to the fact that the doped silver trapped photogenerated electrons and promoted the formation of Ti^{3+} and, hence, the inhibition of the recombination of electron–hole pairs. The probable pathway of PCP mineralization was mainly a surface charge process, caused by adsorbed •OH radicals ($•OH_{ads}$), valence band holes (h_{vb}^+) and electrons (e_{cb}^-), which was verified by studying the effects of scavengers and nitrogen purging.

1. Introduction

For decades, titania (TiO_2) photocatalysis has been investigated as a promising technology for the destruction of various organic contaminants. However, the application of a photocatalytic material has some drawbacks, such as low quantum efficiency and restriction to short-wavelength excitation [1]. Considerable effort has been expended on attempts to enhance the photocatalytic efficiency and visible-light utilization of TiO_2. It is anticipated that doping TiO_2 with appropriate metals and/or non-metals will introduce new energy levels in the band gap of TiO_2 that will extend the photoresponsiveness into the visible-light region and modify the properties of TiO_2 particles to intensify the separation of electron–hole pairs [2–5], and thereby result in visible-light-sensitive photocatalysts. Recently, iodine-doped TiO_2 (I-TiO_2) has been the subject of intensive photocatalyst research. Several groups have reported the visible-light-induced photocatalytic activity of I-TiO_2 [6–9], and TiO_2 co-doped with iodine and rare earth elements [10,11], in which the action of iodine reduces the band gap energy by forming doping levels in the band gap of TiO_2, and acts as a conduction band electron scavenger, retarding the rapid recombination of electron–hole pairs [8], and enhancing the photocatalytic activity to some extent.

Modification of TiO_2 by deposition of noble metals, such as platinum, gold and silver [12–14], induces superior photocatalytic activity, because electrons migrate from TiO_2 to the vicinity of metal particles on the surface, facilitating charge separation that inhibits the recombination of photogenerated electron–hole pairs [15]. In addition, modification of TiO_2 by means of noble metal ion doping can increase the photocatalytic efficiency of TiO_2 [16,17]. Silver has higher work function than TiO_2 and thus electrons photogenerated in TiO_2 tend to migrate to the silver surface. These electrons could react with surface Ti^{4+} to afford surface reactive centers of Ti^{3+}, which is a donor for n-type TiO_2 [18–20]. The higher the donor density for TiO_2, the faster is the photocatalytic degradation rate [21], so it is expected that silver modification could improve the catalytic activity of I-TiO_2. It has been reported that silver particles can promote electron excitation by creating a local electric field, extending the wavelength response towards the visible-light region, and presenting a reasonable enhancement of the electric field due to the surface plasmon resonance effect of metallic silver particles [22,23]. Similarly, the silver ion has a high redox potential and is easily reduced to metallic silver by photoexcited electrons, inhibiting the recombination of electron–hole

* Corresponding author. Tel.: +86 571 88320726; fax: +86 571 88320276.
E-mail address: ss@zjut.edu.cn (S. Song).

1381-1169/$ – see front matter © 2009 Elsevier B.V. All rights reserved.
doi:10.1016/j.molcata.2009.12.003

pairs [24]. Overall, silver has been well studied because of its excellent electrical and thermal conductivity, high degree of stability under ambient conditions, and relatively low cost [25]. However, to our knowledge, there are few systematic descriptions of the synergy effect of Ag combined with I-TiO_2 under visible-light irradiation.

The primary objective of this work was to synthesize and characterize Ag^+-doped I-TiO_2 photocatalysts (Ag-I-TiO_2). The effects of Ag doping on the crystallization and phase transition of TiO_2 nanoparticles as well as the valence distribution of titanium and iodine were elucidated. We evaluated the photocatalytic activity of Ag-I-TiO_2 in the degradation of *p*-chlorophenol (PCP) under visible-light irradiation. Finally, we propose a possible active species using several scavengers and N_2 purging.

PCP was chosen as a model pollutant because it is in widespread use as an intermediate in the synthesis of the higher chlorinated congeners, certain dyes and pesticides, which show low levels of biodegradability and pose serious risks to the environment as persistent organic contaminants in wastewater [26].

2. Experimental

2.1. Materials and reagents

All chemicals were of reagent grade or higher and were used as received. Iodic acid (HIO_3), tetrabutyl titanate ($(C_4H_9O)_4Ti$), and silver nitrate ($AgNO_3$) were purchased from Huadong Medicine Co., Ltd., China. Sodium nitrite ($NaNO_2$) and PCP were obtained from Shanghai Jingchun Reagent Co., Ltd., China. Sodium fluoride (NaF), potassium iodide (KI) and potassium persulfate ($K_2S_2O_8$) used as scavengers were purchased from Huadong Medicine Co., Ltd., China. Nitrogen (purity 99.99%) was provided by Hangzhou Jingong Special Gas Co., Ltd., China. Deionized, doubly distilled water was used throughout this study.

2.2. Preparation and characterization of the photocatalyst

The synthesis of Ag-I-TiO_2 began by dissolving 2.64 g of HIO_3 in 80 mL of water, and then 51 mL of tetrabutyl titanate was added dropwise with continuous stirring. After that, 50 mM $AgNO_3$ was added slowly with vigorous stirring for 2 h to give final atomic ratios of Ag/Ti of 0.5%, 3% and 5%. After air-drying at 80 °C, the precursors were calcined in a furnace (CWF1100, CARBOLITE, England) from room temperature to 400 °C at a heating rate of 5 °C/min, kept at that temperature for 2 h and then allowed to cool to room temperature. The preparation of I-TiO_2 and Ag-TiO_2 powders was as described above except for the addition of HIO_3 or $AgNO_3$, respectively.

The crystalline catalysts were examined by X-ray diffraction (XRD) with a Thermo ARL SCINTAG X'TRA diffractometer at room temperature using Cu Kα irradiation at 45 kV and 40 mA. Crystal sizes were estimated by the Debye–Scherrer equation. Specific surface areas of the samples were determined by measurement of the nitrogen adsorption–desorption isotherm at 77 K using the Brunauer–Emmett–Teller (BET) method with a Micromeritics ASAP 2010 analyser. The transmission electron micrographs (TEM) and the selected area electron diffraction (SAED) micrographs were taken with a Tecnai G2 F30 S-Twin microscope operating at an accelerating voltage of 300 kV with 0.2 nm point resolution. X-ray photoelectron spectroscopy (XPS) experiments were done with an RBD upgraded PHI-5000C ESCA system (PerkinElmer) with Mg Kα radiation (1253.6 eV). The binding energies of Ag, Ti and I were calibrated by using the containment carbon (C 1s = 284.6 eV). Data were analysed with XPSPEAK4.1 software provided by Raymund W.M. Kwok (The Chinese University of Hong Kong, China). In addition, UV–vis diffuse reflectance spectra were measured at room temperature with a UV–vis spectrometer (Spectro UV-2500).

2.3. Photocatalytic activity measurement

Photocatalytic experiments were done in a cylindrical Pyrex glass reactor (diameter, 16 cm; height, 20 cm; total capacity, 3 L) containing 1.5 L of 0.25 mM PCP and 1.5 g of the photocatalyst. The stable aqueous solution was stirred with a magnetic follower and irradiated with a 400 W dysprosium lamp (Beijing Electric Light Sources Research Institute, Beijing, China), which was immersed in 1 L of 2 M $NaNO_2$ as a filter for visible light. The spectrum distribution of the lamp reached level B of the general specification for solar simulators [27]. A port at the top of the photoreactor was used for measuring temperature and for withdrawing samples. During the reactions, a water-jacketed system controlled by a thermostat (THD-2015, Tianheng Instrument Factory, Ningbo, China) was used to maintain the temperature of the PCP solution at 22 (±1) °C and that of the filter solution at 55 (±1) °C. The operating conditions of the thermostat were: capacity, 15 L; flow-rate, 6 L/min; temperature, 5 °C.

For the scavenger experiments, 10-fold (with respect to initial PCP concentration) scavengers were introduced into the PCP solution before the catalyst. In the N_2 purging experiments, cylindrical nitrogen gas diffusers with coarse porosity were placed at the bottom of the reactor. The flow-rate of the nitrogen gas was controlled by a rotameter at 0.08 m^3/h. Nitrogen gas was supplied for 30 min before the experiments in order to obtain the desired oxygen level. During the experiments, 5 mL samples were withdrawn at predetermined time-points and then centrifuged and filtered through a 0.45 μm pore size membrane filter to remove the catalyst particles.

2.4. Sample analysis

All samples were analysed immediately to ensure no further reaction occurred. The concentration of PCP and aromatic intermediates in the reaction solution was monitored by high-pressure liquid chromatography (HPLC) using an Agilent instrument (1200 series, Agilent, USA). Samples (5 μL) were injected onto the column to determine the concentration of PCP, using a mobile phase of acetic acid/acetonitrile/water (1:35:64, by vol). The decrease of total organic carbon (TOC) in the reaction solution, which confirmed the degree of photomineralization of PCP in the reaction solution, was measured with a TOC-V_{CPH} total organic carbon analyser (Shimadzu, Kyoto, Japan).

3. Results and discussion

3.1. Catalyst characterization

The wide-angle XRD analysis of the I-TiO_2 catalyst and 0.5%, 3% and 5% Ag-I-TiO_2 catalysts are shown in Fig. 1. All of the samples clearly revealed the diffraction from the (1 0 1), (0 0 4), (2 0 0), (1 0 5), (2 0 4) planes of anatase titania and the (1 2 1) planes of brookite. It was noted that the weak (1 1 0) plane of the rutile phase appeared on Ag-doped samples. The rutile phase usually appears at temperature >400 °C; the analytical results showed that the presence of silver enhances the thermodynamically feasible anatase to rutile phase transformation. This is ascribed to an increase of the density of surface defects as well as the surface oxygen vacancy concentration, which both favour this phase transformation [28,29].

The prepared catalysts crystallized predominantly in the anatase phase. We found that the relative intensity of (1 0 1) peaks was attenuated and broadened with increasing Ag content, indicating that the Ag doping inhibits the growth of anatase grains and the

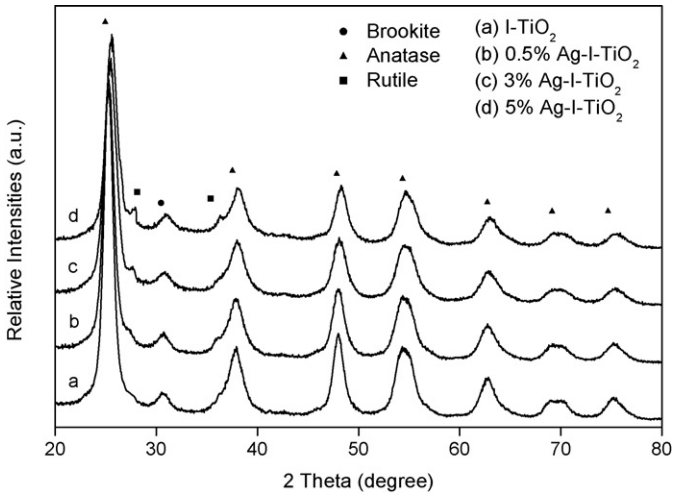

Fig. 1. XRD patterns of I-TiO_2 and Ag-I-TiO_2 with 0.5%, 3% and 5% of Ag-doped.

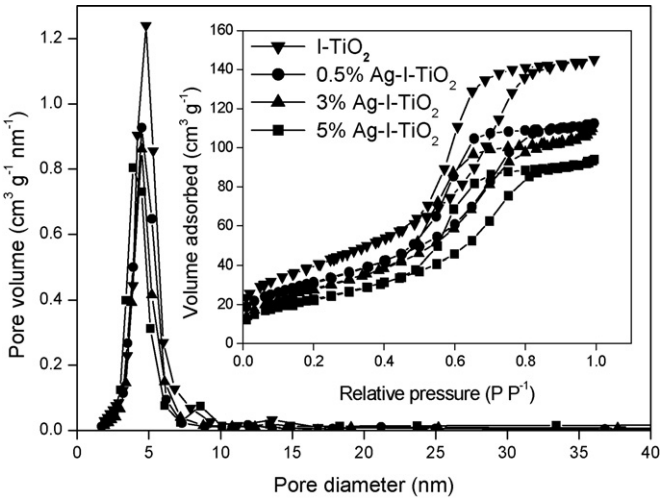

Fig. 2. Nitrogen adsorption–desorption isotherms (inset) and pore size distribution of I-TiO_2 and 0.5%, 3% and 5% of Ag-I-TiO_2.

formation of crystallites [30,31]. The fraction of anatase phase calculated from the quantitative expressions was 83.3%, 82.6%, 80.2% and 78.2%, respectively [32]. Additionally, the crystallite sizes calculated from XRD peaks of the crystal plane (1 0 1) in anatase were decreased from 6.57 nm to 5.27 nm, as estimated from the Debye–Scherrer equation (Table 1). Unfortunately, the diffraction peaks that could be assigned to the planes of the Ag species, either Ag^0 or Ag^+, were inconspicuous. This might be due to the low content or the amorphous state of Ag [33]. Besides, the intensity of the Ag peaks might be overlapped by those of TiO_2. For instance, the peak at 37.8° related to the anatase (2 0 0) orientation is very close to the peak at 38.2° corresponding to Ag (1 1 1) [34,35].

The lattice parameters *a* and *c* were determined before and after doping with Ag. The results in Table 1 show that the values of *a* and *c* were reduced with increasing Ag content, suggesting the distortion of the crystal lattice as a result of Ag addition. There are two possible sites for the element Ag in the TiO_2 crystal structure: located in the grain boundary layers or embedded in the matrix. For Ag modification, it is well accepted that metallic Ag^0 should be deposited onto the surface of TiO_2. Nevertheless, the location of Ag^+ is still controversial. Some researchers are convinced that, from the point of view of radius matching, Ag^+ cannot enter the TiO_2 lattice because the ionic radius (0.126 nm) is much greater than that of Ti^{4+} (0.068 nm). In this case, the decrease of the lattice parameters should be due to the press of the doped Ag^+ located on the surface vertical to the *c*-axis of the TiO_2 crystal [36]. Others consider that, although it is difficult for Ag^+ to act as an interstitial ion in the TiO_2 lattice because of its larger radius, it could substitute the lattice sites of Ti^{4+}, providing more oxygen vacancies and reducing the TiO_2 lattice [17]. In any case, the introduction of Ag^+ could enhance the photocatalytic activity of TiO_2 to some extent. In our experiments, it is most likely that the Ag^+ are situated around the TiO_2 grain boundary, as discussed below.

The pore structures of samples were characterized by the N_2 adsorption–desorption method. As shown in the inset in Fig. 2, the N_2 adsorption–desorption isotherms of the prepared samples are type IV isotherms with type H2 hysteresis loops for the capillary

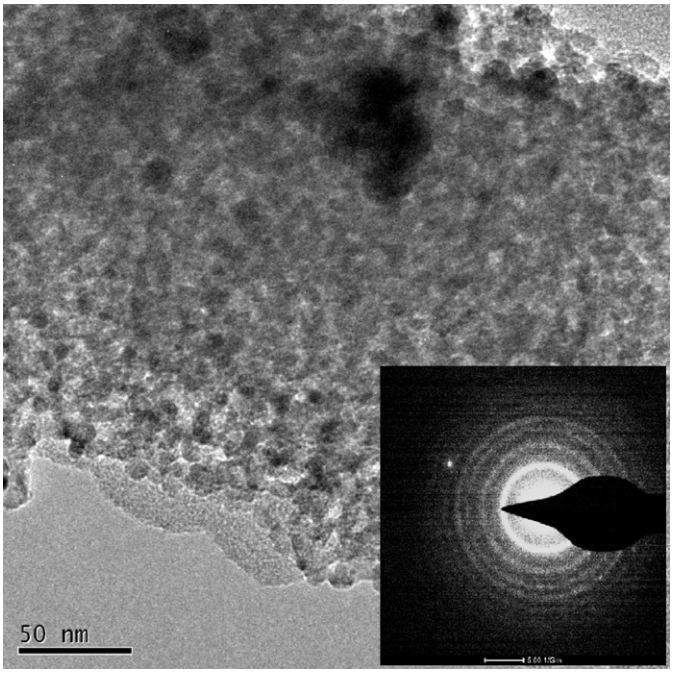

Fig. 3. TEM image and SAED (inset) of Ag-I-TiO_2 (3%).

condensation within the pores, which are characteristics typical of mesoporous materials [37]. Barrett–Joyner–Halenda (BJH) analysis of the pore size distribution from the desorption branch of the isotherm is shown in Fig. 2. The main peaks were observed at ~5 nm with a narrow pore distribution related to the sharp hysteresis loop. The results, including the BET surface area and pore volume, are given in Table 1. With the increase in the amount of doped Ag, the BET surface area decreased from 145.56 m^2/g to 83.62 m^2/g, and the pore volume decreased from 0.224 cm^3/g to 0.145 cm^3/g, respec-

Table 1
Refined structural parameters for the prepared catalysts.

	a (Å)	*c* (Å)	BET surface area (m^2/g)	Pore volume (cm^3/g)	Crystallite size (nm)
I-TiO_2	3.792	9.482	145.6	0.224	6.57
0.5% Ag-I-TiO_2	3.783	9.466	114.2	0.174	6.18
3% Ag-I-TiO_2	3.779	9.434	105.2	0.169	5.77
5% Ag-I-TiO_2	3.760	9.380	83.6	0.145	5.27

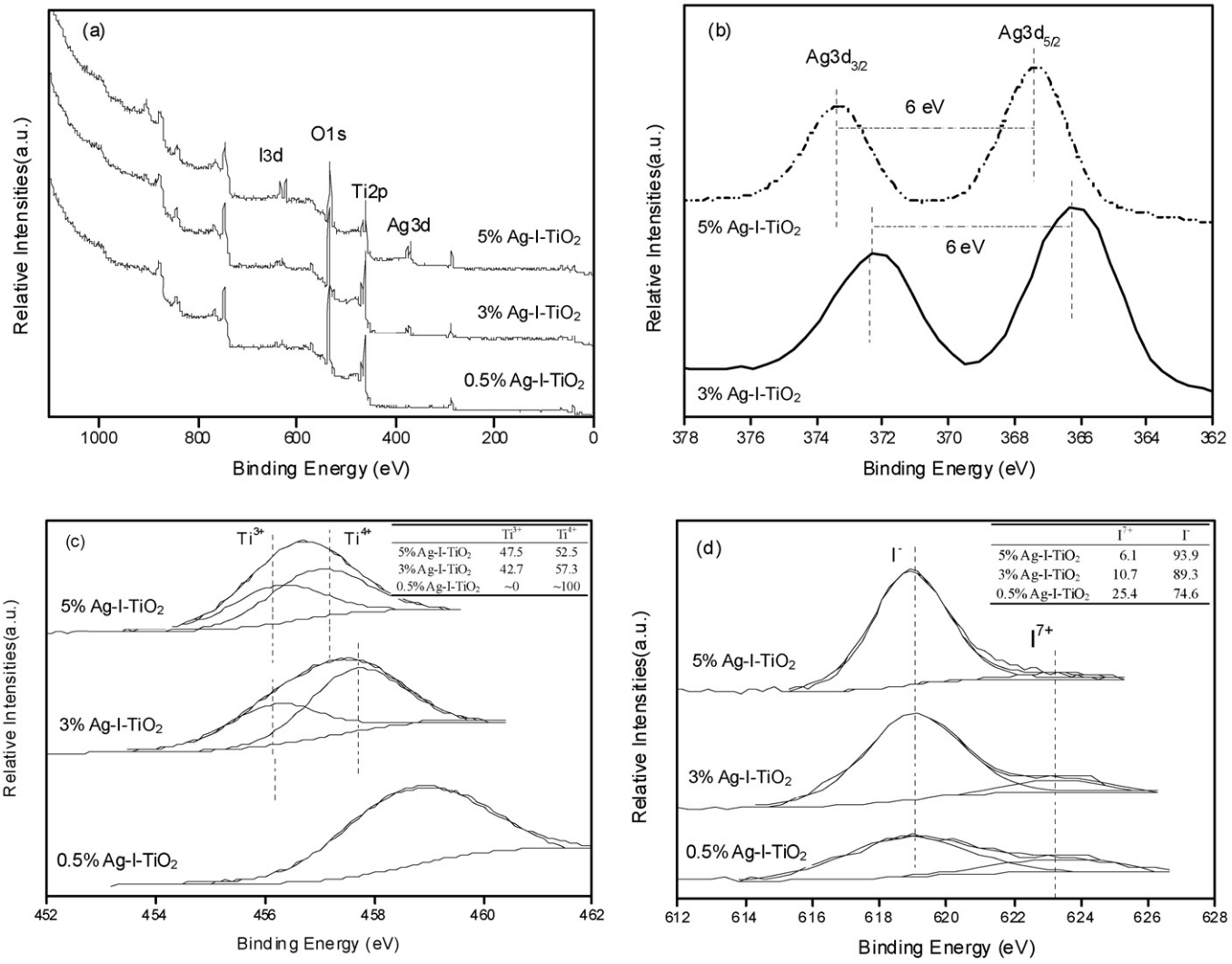

Fig. 4. XPS spectra of a series of as-prepared Ag-I-TiO_2, 0.5%, 3% and 5% of Ag-doped (a), respectively, and XPS spectra in the Ag 3d (b), Ti 2p (c) and I 3d (d) core levels.

tively. The Ag species of our samples should be located around the grain boundary of TiO_2, thus occupying the pores of catalyst particles, and effectively decreasing the BET surface area and the available pore volume.

The microscopic structure of the Ag-I-TiO_2 (3%) catalyst was determined by TEM (see Fig. 3). It is obvious from the mass contrast that the dense particle consisted of well dispersed I-TiO_2 particles, and electron diffraction of SAED from the particles confirms the predomination of the anatase phase in the catalysts. From the inner to the outer, the rings originated from the anatase phase of TiO_2 represented the (1 0 1), (0 0 4), (2 0 0), (1 0 5) and (2 0 4) planes [38]. However, the Ag clusters in the typical image, and the spots attributed to metallic silver were not observed in the corresponding photograph of SAED (Fig. 3, inset) [34,37], implying the absence of Ag^0. Because the XPS findings (see below) show that the Ag species indeed exists in the catalysts, the element Ag might be in the +1 valence state.

XPS measurements were used to elucidate the chemical state of Ag and other species in the Ag-I-TiO_2 composite. The wide-scan XPS spectra for Ag-I-TiO_2 with different contents of Ag show the peaks of binding energy (BE) for C 1s, O 1s, I 3d, Ti 2p and Ag 3d, and the high-resolution XPS spectra of Ti $2p_{3/2}$, I 3d and Ag 3d are shown in Fig. 4. Except the 0.5% sample, in hardly any peak was detected owing to the low Ag content, the Ag 3d XPS of Ag-doped samples are shown in Fig. 4b. The characteristic Ag $3d_{5/2}$ and Ag $3d_{3/2}$ doublet peaks were observed at BE 366.3 eV and 372.3 eV for 3% Ag-I-TiO_2, respectively, while those for 5% Ag-I-TiO_2 are 367.3 eV and 373.3 eV, respectively. It is difficult to define the valence state of Ag unambiguously because of the closely similar binding energy of Ag^+ and Ag^0, as well as the same splitting of 6 eV of the Ag 3d doublet for both of them [39]. Normally, the XPS spectra of Ag $3d_{5/2}$ at 366–368 eV can be assigned to Ag^+ and the values above 368 eV can be attributed to Ag^0 [28,31,40,41]. Thus, the Ag 3d XPS of Ag-doped samples in our experiments should originate from Ag^+. Furthermore, we could deduce the chemical valence of Ag by the synthesis method. No reductant was added during the synthesis of Ag-I-TiO_2 in our experiments. Therefore, it can be inferred that Ag in the precursors might be in the form of $AgIO_3$ and $AgNO_3$ before thermal treatment. The decomposition temperature of $AgIO_3$ is 410 °C and that of $AgNO_3$ is 444 °C [42,43]; therefore, we conclude that Ag is most likely to be in the form of Ag^+ after calcination at 400 °C. Moreover, the molar ratio of Ag/Ti on the surface of Ag-I-TiO_2 obtained from the XPS data (4.6% and 17.3%, respectively) is greater than the doping ratio (3% and 5%, respectively), indicating that the Ag^+ was located on the surface of I-TiO_2 because the XPS analysis is surface-sensitive.

It is surprising that the Ag 3d XPS signals are shifted by 1 eV with increasing Ag doping concentration from 3% to 5%, as shown

in Fig. 4b. This shift might be attributable to the comprehensive electron transformation among the elements in the catalysts. For example, some electrons might be transferred from TiO_2 to Ag, which is ascribed to the interaction between them [40], and cause the negative shift of Ag 3d. Nevertheless, electrons might be transferred from Ag to O because of the larger electronegativity of O [44], resulting in the increase of binding energy of Ag 3d. In any case, such a large shift of Ag 3d in our tests is quite curious and deserves further study.

The spectra in the core level of Ti $2p_{3/2}$ and I 3d are shown in Fig. 4c and d. It can be observed that the Ti $2p_{3/2}$ peak for the catalysts shows a slight deformation on the lower binding energy side, indicative of the different oxidation states of Ti, which were well fitted to the two peaks matching Ti^{3+} and Ti^{4+} in the Ti $2p_{3/2}$ region. A similar outcome has been reported by other researchers [40,45]. The Ti^{3+}/Ti^{4+} ratio increased as the Ag doping increased (see the inset in Fig. 4c) might be because Ag enhances the interaction between I and TiO_2 [9]. In addition, the presence of the Ti^{3+} surface state favours the separation of electron–hole pairs and has important roles in the photo-oxidation of organic compounds on the TiO_2 photocatalyst [6,10].

The XPS spectrum of the I 3d region shows a doublet peak at 618.4 eV and at 623.9 eV, suggesting that I exists in multiple valence forms in the samples. The ascription of the binding energy to I ions is still the subject of dispute [6–9]. For example, the binding energy for I $3d_{5/2}$ observed at 623.9 eV for the Ag-I-TiO_2 samples is much smaller than that reported by Hong et al. [6] (627.5 eV), which was considered to be questionable by Su et al. [9]. In the present work, the doublet peak at 618.4 eV and at 623.9 eV is most probably due to the coexistence of the I^- and I^{7+} species, because iodine is inclined to be stable in the coexistence of IO_4^- and I^- via the disproportionating reaction of IO_3^- [9]. We find that the addition of Ag is advantageous for the interaction between I and TiO_2, since the Ti^{3+}/Ti^{4+} ratio increased with increased Ag level, which is a stimulative factor for the electron–hole separation in the photodegradation of organic compounds on the TiO_2 photocatalysts.

The proportion of I^- was increased along with the increased concentration of Ag. Theoretically, the total amount of elemental iodine is equivalent in all of the samples that were calcined at 400 °C. Since the XPS analysis is surface-sensitive, we deduce that more I^- might diffuse to the surface of TiO_2 accompanied by an increased content of Ag.

The optical absorbance spectra of the Ag-doped and undoped I-TiO_2 photocatalysts measured in the UV–vis region are shown in Fig. 5. It has been reported that the introduction of Ag^+ could expand the absorption edge of TiO_2 to longer wavelengths, owing to the charge transfer transitions between Ag^+ and TiO_2, as well as the creation of oxygen vacancies in the TiO_2 lattice [34]. However, absorbance in the visible light range of 400–475 nm can be mainly assigned to the coexistence of I–O–I and I–O–Ti structures caused by iodine doping in the TiO_2 crystal structure [46]; therefore, the effect of the red shift originating from Ag^+ doping might be inconspicuous until the amount of Ag doping was 5%, as illustrated in Fig. 5.

3.2. Photocatalytic activity

The Ag doping has an important effect on photocatalytic activity. Because of the high redox potential of Ag^+, it is easily reduced to Ag^0 by the photo-excited conduction band electrons, preventing the recombination of electron–hole pairs [24]. However, a greater amount of Ag doping might be detrimental for the photocatalytic activity. To explore the correlation between photocatalytic activity and Ag content, we compared the photocatalytic activity of the degradation of PCP under visible light irradiation using I-TiO_2, Ag-TiO_2 (3%) and Ag-I-TiO_2 with a Ag content of 0.5%, 3% and 5% as

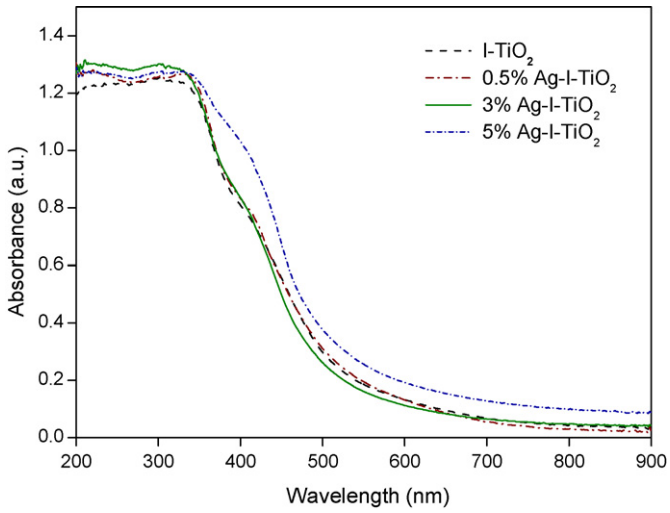

Fig. 5. UV–visible diffuse reflectance spectra of I-TiO_2 and 0.5%, 3% and 5% of Ag-I-TiO_2 powders.

catalysts. Fig. 6a and b shows the efficiency of the photocatalytic conversion of PCP and the removal of TOC after 240 min. Compared to I-TiO_2 and Ag-TiO_2 (3%), the photocatalytic activity was enhanced markedly owing to the synergistic effect of Ag and I. The photocatalytic activity of Ag-I-TiO_2 increased with increasing Ag content up to 3% (the optimum metal doping level) and then decreased, and the TOC that was used to prove the total mineralization of PCP had a similar trend.

The standard potential of Ag^+ is suitable for trapping electrons from the TiO_2 conduction band to form Ag^0 on the TiO_2 surface, acting as electron–hole separation centers in the photocatalytic reaction process. Thus, doping Ag^+ improved the photocatalytic activity of I-TiO_2 effectively. Moreover, during the photocatalytic

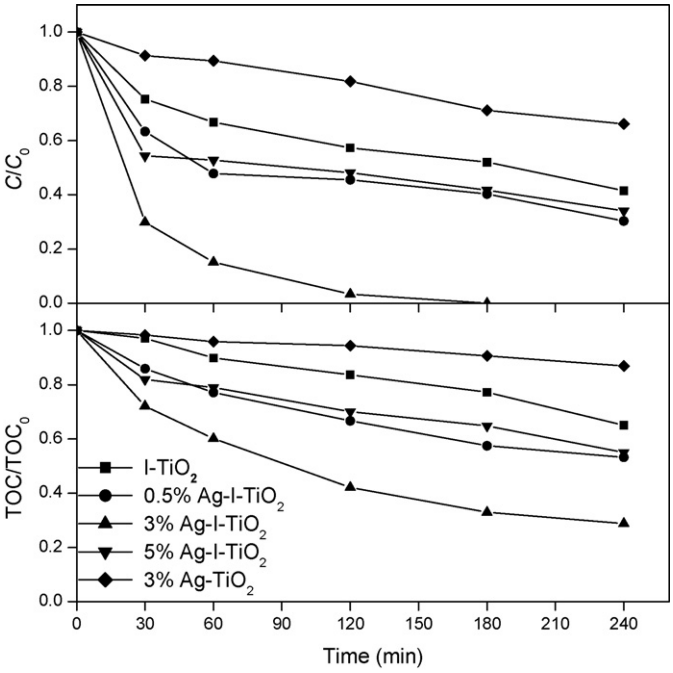

Fig. 6. Comparison of the change of concentration of PCP (a) and the TOC removal (b) in the presence of I-TiO_2, Ag-TiO_2 (3%) and Ag-I-TiO_2 with 0.5%, 3% and 5% of Ag-doped, respectively, under visible light illumination. Experimental conditions: initial concentration of PCP, 0.25 mM; photocatalyst dose, 1.0 g/L; bulk temperature, 22 °C; air equilibrium.

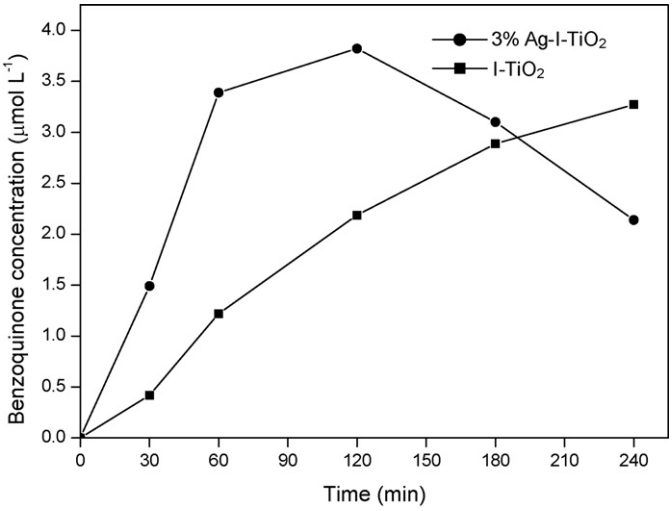

Fig. 7. Variation of the concentration of the intermediate benzoquinone with time. Experimental conditions: initial concentration of PCP, 0.25 mM; photocatalyst dose, 1.0 g/L; bulk temperature, 22 °C; air equilibrium.

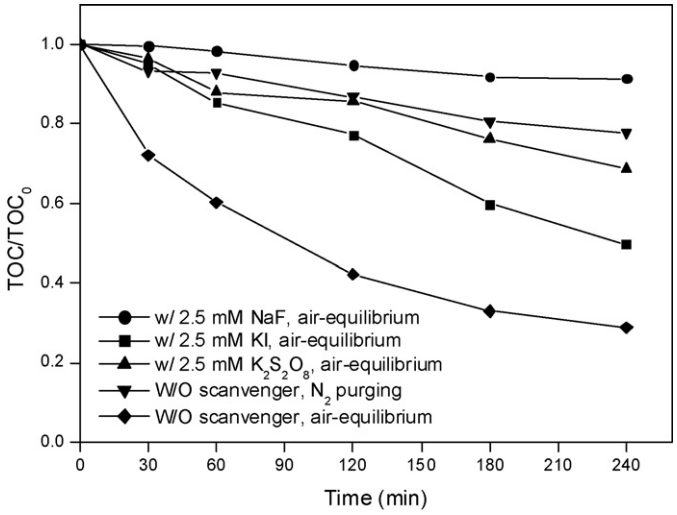

Fig. 8. The efficiency of TOC reduction in the presence of Ag-I-TiO_2 (3%) under visible light irradiation with/without scavengers in an air equilibrium system, and without scavengers in a N_2-purged system. Experimental conditions: initial concentration of PCP, 0.25 mM; 10-fold scavengers; photocatalyst dose, 1.0 g/L; bulk temperature, 22 °C.

reaction, photogenerated electrons can be trapped by molecular oxygen or surface Ti^{4+}, stimulated by Ag^+ on the surface, to generate reactive $O_2^{\bullet-}$ and surface Ti^{3+}, respectively [19,47,48], further enhancing the consequent separation of electron–hole pairs. Thus, the Ti^{3+}/Ti^{4+} ratio would increase with an increase in silver doping in this case. However, if the Ag content was greater than its optimum value, the negative charge accumulated on the Ag would be combined with the hole again, decreasing the efficiency of the photocatalytic activity. Furthermore, the Ag metallic particles, originated from Ag^+ reduction, on the surface might act as a barrier, preventing light absorption and weakening the radiancy of the TiO_2 surface and, hence, reducing the production of electron–hole pairs [1]. An analogous negative behaviour was observed when other metals, such as La and Fe, were incorporated into TiO_2 [49,50]. Taken together, the results presented above indicate that 3% is the optimum Ag content (see Fig. 6).

Determination of the major intermediates formed during the photocatalytic process is helpful in obtaining further insight into the reaction mechanism. HPLC was used to analyze quantitatively the intermediates involved in PCP photodegradation. The main aromatic intermediates in PCP degradation include benzoquinone, hydroquinone, hydroxyhydroquinone and 4-chlorocatechol [51–53]. However, our results showed that benzoquinone was the only measurable aromatic intermediate. This may be because the decomposition rate of undetected intermediates is higher than their formation rate and thus concentrations of these intermediates would be below detectable limits [51]. As shown in Fig. 7, within 4 h of reaction, the concentration of benzoquinone for Ag-I-TiO_2 with 3% Ag initially increased and then decreased, whereas that for I-TiO_2 did not reach a maximum, further demonstrating the effectiveness of silver in enhancing the photocatalytic activity.

3.3. Dominant reactants during the mineralization of PCP

Various active species exist in photoreaction systems, but it is generally considered that the TiO_2 photocatalytic reactions are always initiated by the valence band hole (h_{vb}^+) or the adsorbed OH radical ($^{\bullet}OH_{ads}$) [54]. The approach of active species generated via the electroreduction of dissolved oxygen with photogenerated conduction band electrons (e_{cb}^-) has obtained increasing attention [55], including studies of the free OH radical ($^{\bullet}OH_{free}$), superoxide ions ($O_2^{\bullet-}$), hydrogen peroxide radicals ($HO_2^{\bullet}$) and hydrogen peroxide (H_2O_2). Three main reaction pathways in the TiO_2 photocatalytic processes are discussed with reference to the different actions of the primary species. If the reaction is caused principally by hydroxyl radicals ($^{\bullet}OH_{ads}$ and/or $^{\bullet}OH_{free}$), it is called an $^{\bullet}OH$ mechanism; if valence band holes (h_{vb}^+) act as the main oxidant in the reaction, the pathway is called a hole mechanism [54]; and the reaction that occurs with the electron is called the mechanism of the electron pathway [55]. Essentially, the destruction of TOC is the ultimate goal of all advanced oxidation processes; thus, to systematically determine the pathway used during the mineralization of PCP using Ag-I-TiO_2 catalysts, the influence of different scavengers and N_2 purging on the rate of mineralization of PCP were investigated and the results are shown in Fig. 8.

Fluoride is adsorbed strongly onto the surface of TiO_2 catalysts to form the F–Ti bond [56]. Thus, the PCP adsorbed on the surface of TiO_2 was almost completely replaced by F^-. The rate of TOC removal of PCP was inhibited strongly by the presence of 2.5 mM NaF, implying that the mineralization of PCP is a surface charge process in which adsorption is preferential on the surface of catalysts before mineralization. Furthermore, the rate of mineralization of PCP was decreased moderately when 2.5 mM KI was used as a scavenger to react with h_{vb}^+ and $^{\bullet}OH_{ads}$ over the catalyst surface [57], suggesting that the h_{vb}^+ mechanism and/or the $^{\bullet}OH_{ads}$ mechanism are effective for the mineralization of PCP.

Molecular oxygen usually acts as an acceptor of photoelectrons in heterogeneous photocatalysis [58]. The solution with Ag-I-TiO_2 suspensions purged with N_2, which decreased the dissolved oxygen level from 0.15 mM to 0.01 mM, had a remarkably lower rate of TOC removal than that in the air-equilibrated solution. This indicates that oxygen cannot be discounted for the mineralization of PCP, and confirms the significance of the electron pathway because many of the active species ($O_2^{\bullet-}$, $HO_2^{\bullet}$, H_2O_2, $^{\bullet}OH_{free}$) can be generated from the electroreduction of dissolved oxygen [55]. A further experiment of PCP mineralization was done using the more efficient e_{cb}^- acceptor $K_2S_2O_8$ [59]. The results reveal that 2.5 mM $K_2S_2O_8$ had a marked restraint on the TOC removal of PCP, showing that the e_{cb}^- pathway is also effective for the mineralization of PCP.

In summary, according to the effect of the scavengers as well as N_2 purging, mineralization of PCP occurred mostly on the surface of Ag-I-TiO_2 catalysts by three main pathways, attributed to the action of h_{vb}^+, $^{\bullet}OH_{ads}$ and e_{cb}^-.

4. Conclusions

A series of Ag-I-TiO_2 photocatalysts were prepared, characterized and tested for activity. The Ag-I-TiO_2 catalyst with a 3% Ag content exhibited more efficient photocatalytic activity than I-TiO_2 in the degradation of PCP under visible light irradiation. The superiority of the Ag-I-TiO_2 photocatalyst was attributed to the fact that the Ag^+ doping can effectively slow the recombination of the e_{cb}^-–h_{vb}^+ pairs via the formation of Ag^0 on the surface of the catalyst, and the favourableness of the Ti^{3+} formed.

Since a loss of dopant atoms could change the photocatalytic activity [60], further work is required to determine how to avoid silver or iodine leaching to maintain the long-term stability of Ag-I-TiO_2 photocatalysts. In any case, we have presented a method for extending the photocatalytic activity of TiO_2 toward the visible light region. An in-depth study is required for the application of these novel photocatalysts in the degradation of other organic species utilizing solar energy.

Acknowledgements

This work was supported by the National Natural Science Foundation of China (Grant No. 20977086), National Basic Research Program of China (Grant No. 2009CB421603), and Zhejiang Provincial Natural Science Foundation of China (Grant Nos. Z5080207 and R5090033). The authors are grateful to Dr. Anyuan Yin from Fudan University for his kind help with the XPS measurements.

References

[1] X.G. Hou, M.D. Huang, X.L. Wu, A.D. Liu, Chem. Eng. J. 146 (2009) 42–48.
[2] R. Asahi, T. Morikawa, T. Ohwaki, K. Aoki, Y. Taga, Science 293 (2001) 269–271.
[3] H. Irie, Y. Watanabe, K. Hashimoto, J. Phys. Chem. B 107 (2003) 5483–5486.
[4] T. Umebayashi, T. Yamaki, H. Itoh, K. Asai, Appl. Phys. Lett. 81 (2002) 454–456.
[5] T. Sano, S. Kutsuna, N. Negishi, K. Takeuchi, J. Mol. Catal. A: Chem. 189 (2002) 263–270.
[6] X.T. Hong, Z.P. Wang, W.M. Cai, F. Lu, J. Zhang, Y.Z. Yang, N. Ma, Y.J. Liu, Chem. Mater. 17 (2005) 1548–1552.
[7] G. Liu, Z.G. Chen, C.L. Dong, Y.N. Zhao, F. Li, G.Q. Lu, H.M. Cheng, J. Phys. Chem. B 110 (2006) 20823–20828.
[8] S. Tojo, T. Tachikawa, M. Fujitsuka, T. Majima, J. Phys. Chem. C 112 (2008) 14948–14954.
[9] W.Y. Su, Y.F. Zhang, Z.H. Li, L. Wu, X.X. Wang, J.Q. Li, X.Z. Fu, Langmuir 24 (2008) 3422–3428.
[10] Z.Q. He, X. Xu, S. Song, L. Xie, J.J. Tu, J.M. Chen, B. Yan, J. Phys. Chem. C 112 (2008) 16431–16437.
[11] S. Song, J.J. Tu, L.J. Xu, X. Xu, Z.Q. He, J.P. Qiu, J.G. Ni, J.M. Chen, Chemosphere 73 (2008) 1401–1406.
[12] S. Chavadej, P. Phuaphromyod, E. Gulari, P. Rangsunvigit, T. Sreethawong, Chem. Eng. J. 137 (2008) 489–495.
[13] G. Zhao, H. Kozuka, T. Yoko, Thin Solid Films 277 (1996) 147–154.
[14] H.M. Sung-Suh, J.R. Choi, H.J. Hah, S.M. Koo, Y.C. Bae, J. Photochem. Photobiol. A: Chem. 163 (2004) 37–44.
[15] A.L. Linsebigler, G.Q. Lu, J.T. Yates, Chem. Rev. 95 (1995) 735–758.
[16] S. Kim, S.J. Hwang, W.Y. Choi, J. Phys. Chem. B 109 (2005) 24260–24267.
[17] Y. Liu, C.Y. Liu, Q.H. Rong, Z. Zhang, Appl. Surf. Sci. 220 (2003) 7–11.
[18] R. Tongpool, K. Setwong, Chiang Mai J. Sci. 35 (2008) 274–282.
[19] Y.S. Cao, H.H. Tan, T.Y. Shi, T. Tang, J.Q. Li, J. Chem. Technol. Biotechnol. 83 (2008) 546–552.
[20] D.S. Kong, Langmuir 24 (2008) 5324–5331.
[21] G.L. Huang, S.C. Zhang, T.G. Xu, Y.F. Zhu, Environ. Sci. Technol. 42 (2008) 8516–8521.
[22] E. Bae, W. Choi, Environ. Sci. Technol. 37 (2003) 147–152.
[23] M.K. Seery, R. George, P. Florisa, S.C. Pillaib, J. Photochem. Photobiol. A: Chem. 189 (2007) 258–263.
[24] B. Ohtani, Y. Okugawa, S. Nishimoto, T. Kagiya, J. Phys. Chem. 91 (1987) 3550–3555.
[25] X. He, X. Zhao, B. Liu, J. Non-Cryst. Solids 354 (2008) 1267–1271.
[26] Y.X. Du, M.H. Zhou, L.C. Lei, J. Hazard. Mater. 139 (2007) 108–115.
[27] State Bureau of Quality and Technical Supervision of China. General specification for solar simulator. National Technical Standard of China GB/T12637-90.
[28] B.F. Xin, L.Q. Jing, Z.Y. Ren, B.Q. Wang, H.G. Fu, J. Phys. Chem. B 109 (2005) 2805–2809.
[29] J.M.G. Amores, V.S. Escribano, G. Busca, V. Lorenzelli, J. Mater. Chem. 4 (1994) 965–971.
[30] C. He, Y. Yu, X.F. Hu, A. Larbot, Appl. Surf. Sci. 200 (2002) 239–247.
[31] M.S. Park, M. Kang, Mater. Lett. 62 (2008) 183–187.
[32] H.Z. Zhang, J.F. Banfield, J. Phys. Chem. B 104 (2000) 3481–3847.
[33] H. Zhang, G. Wang, D. Chen, X.J. Lv, U.H. Jinghong, Chem. Mater. 20 (2008) 6543–6549.
[34] R. Vinu, G. Madras, Appl. Catal. A: Gen. 366 (2009) 130–140.
[35] O. Akhavan, E. Ghaderi, Surf. Coat. Int. 203 (2009) 20–21.
[36] X.W. Wu, D.J. Wu, X.J. Liu, Chin. Phys. Lett. 26 (2009), 077809-1-4.
[37] Y. Liu, X.L. Wang, F. Yang, X.R. Yang, Micropor. Mesopor. Mater. 114 (2008) 431–439.
[38] L. Miao, Y. Ina, S. Tanemura, T. Jiang, M. Tanemura, K. Kaneko, S. Toh, Y. Mori, Surf. Sci. 601 (2007) 2792–2799.
[39] J.F. Moulder, W.F. Stickle, P.E. Sobol, K.D. Bomben, Handbook of X-ray Photoelectron Spectroscopy, 2nd ed., PerkinElmer Corp., Waltham, MA, 1992.
[40] S. Rengaraj, X.Z. Li, J. Mol. Catal. A: Chem. 243 (2006) 60–67.
[41] J.X. Li, J.H. Xu, W.L. Dai, K.N. Fan, J. Phys. Chem. C 113 (2009) 8343–8349.
[42] T. Fukasawa, K. Funabashi, Y. Kondo, J. Nucl. Sci. Technol. 31 (1994) 1073–1083.
[43] Z.H. Yuan, W. Zhou, Y.Q. Duan, L.J. Bie, Nanotechnology 19 (2008), 075608-1-5.
[44] H.P. He, Y.X. Wang, H.W. Chen, Solid State Ionics 175 (2004) 651–654.
[45] K. Schwanitz, U. Weiler, R. Hunger, T. Mayer, W. Jaegermann, J. Phys. Chem. C 111 (2007) 849–854.
[46] G. Liu, C.H. Sun, X.X. Yan, L. Cheng, Z.G. Chen, X.W. Wang, L.Z. Wang, S.C. Smith, G.Q. Lu, H.M. Cheng, J. Mater. Chem. 19 (2009) 2822–2829.
[47] M.I. Litter, Appl. Catal. B: Environ. 23 (1999) 89–114.
[48] S.X. Liu, Z.P. Qu, X.W. Han, C.L. Sun, Catal. Today 93–95 (2004) 877–884.
[49] Y.Q. Wang, H.M. Cheng, L. Zhang, Y.Z. Hao, J.M. Ma, B. Xu, W.H. Li, J. Mol. Catal. A: Chem. 151 (2000) 205–216.
[50] C.Y. Wang, D.W. Bahnemann, J.K. Dohrmann, Chem. Commun. 16 (2000) 1539–1540.
[51] G. Sivalingam, M.H. Priya, G. Madras, Appl. Catal. B: Environ. 51 (2004) 67–76.
[52] A. Mills, S. Morris, R. Davies, J. Photochem. Photobiol. A: Chem. 70 (1993) 183–191.
[53] Y.P. Cheng, H.Q. Sun, W.Q. Jin, N.P. Xu, Chem. Eng. J. 128 (2007) 127–133.
[54] S.H. Yoon, S.E. Oh, J.E. Yang, J.H. Lee, M. Lee, S. Yu, D. Pak, Environ. Sci. Technol. 43 (2009) 864–869.
[55] P. Salvador, J. Phys. Chem. C 111 (2007) 17038–17043.
[56] C. Minero, G. Mariella, V. Maurino, D. Vione, E. Pelizzetti, Langmuir 16 (2000) 8964–8972.
[57] S.T. Martin, A.T. Lee, M.R. Hoffmann, Environ. Sci. Technol. 29 (1995) 2567–2573.
[58] S. Song, L.J. Xu, Z.Q. He, J.M. Chen, X.Z. Xiao, B. Yan, Environ. Sci. Technol. 41 (2007) 5846–5853.
[59] Y.B. Wang, C.S. Hong, Water Res. 33 (1999) 2031–2036.
[60] M.M. Kondo, W.F. Jardim, Water Res. 25 (1991) 823–827.